Evaluation of the effective potential barrier height in nonlinear magnetization dynamics excited by ac magnetic field

Genki Okano[1] and Yukio Nozaki[1,2,*]

[1]*Department of Physics, Keio University, Yokohama 223-8522, Japan*

[2]*Center for Spintronics Research Network, Keio University, Yokohama 223-8522, Japan*

(Received 23 October 2017; published 26 January 2018)

An alternating current (ac) magnetic field or spin current can reduce the switching field of a ferromagnet through resonance excitation of a large-angle precession of magnetization. The nonlinear magnetization dynamics of this switching scheme completely differ from the general ferromagnetic resonance phenomenon, which is linearly excited by a small ac magnetic field. To understand these dynamics, it is necessary to evaluate the effective potential barrier height for switching, ΔU^{eff}. However, most previous studies have measured the consequent precession angle in the nonlinear dynamics by magneto-optical methods and/or by applying a magneto-resistive effect. Here, we applied the cooperative switching method, which evaluates the ΔU^{eff} of the nonlinear dynamics under a sub-ns-wide magnetic field impulse, and observed a nontrivial reduction of ΔU^{eff} in a submicron-wide NiFe strip. The strong reduction of ΔU^{eff} under a negative magnetic field was caused by a saddle-node bifurcation in the nonlinear dynamics. In a micromagnetics simulation, we also confirmed that the magnetization is nonuniformly excited at the shallowest ΔU^{eff}.

DOI: 10.1103/PhysRevB.97.014435

I. INTRODUCTION

Under a strong alternating current (ac) magnetic field H_{ac} or a spin current, the magnetization dynamics of a ferromagnet are excited in a nonlinear manner. A recent numerical study suggests that strongly excited magnetization dynamics show a variety of nonlinear and chaotic phenomena [1]. Such nonlinear excitation promises to reduce the switching fields of ferromagnets with ultrastrong magnetic anisotropy energies. Since frequency-dependent reduction of the switching field was experimentally demonstrated in a single-crystalline Co nanoparticle [2], microwave-assisted magnetization switching (MAS) has been widely investigated in microfabricated ferromagnetic thin films with in-plane [3–7] and perpendicular magnetic anisotropy [8–18]. In microwave-assisted magnetic recording (MAMR), a spin-torque oscillator is embedded in the writing head of a hard disk drive [19–21]. The oscillator generates an ac magnetic field that reduces the amplitude of the recording field.

Most of the experimental MAS studies have investigated the reduction of the critical switching field under H_{ac} with varying amplitudes and frequencies. When the ac magnetic field is orthogonally applied to the magnetization precession axis in the laboratory frame, it induces an inertial direct current (dc) magnetic field in a rotating frame that opposes the initial magnetization direction. Moreover, as the amplitude of the negatively applied inertial magnetic field is proportional to both the amplitude and frequency of H_{ac}, the switching field is reduced. However, a simple analysis using a macrospin model also predicts that an additional torque acts on the magnetization and suppresses the precession angle [22,23]. The amplitude of the torque increases with the frequency of H_{ac} and it leads to an increment of the switching field above a critical frequency. Indeed, the critical behavior predicted by the simple macrospin model can explain the observed nonlinear magnetization dynamics in MAS experiments of small magnetic particles. On the other hand, when the lateral size and thickness of the ferromagnetic body are larger than the exchange length [24] (given by $l_{\text{ex}} = \sqrt{A/(2\pi M_s^2)}$, where A is the exchange constant and M_s is the saturation magnetization), the critical condition for magnetization switching depends on nonuniformly excited magnetization precession, such as spin waves [8]. Under these conditions, the macrospin model no longer captures the amplitude and frequency threshold behaviors in MAS experiments. In magnetic recording research, an exchange-coupled composite (ECC) medium [25–30] promises to increase the areal recording density while ensuring sufficient thermal stability and decreasing the recording field. The ECC medium constitutes two or more ferromagnetic thin films with different perpendicular anisotropies stacked along the thickness direction. To realize MAMR in a synthetic ECC medium, one should understand the influences of the nonuniform excitation.

The existence condition of the metastable switching states below the critical H_{ac} are especially important, because it prevents deterministic MAS. The switching scheme in MAS is largely governed by nonlinear effects such as complicated bifurcation in the switching phase diagram [31–34], nonuniform excitation caused by magnon scattering, and saturation of the precession angle [35–38]. Bertotti *et al.* studied the bifurcation [31–33] in the switching phase diagram as a function of orthogonal H_{ac} amplitude, fixing the H_{ac} frequency and applying a negative static field H_{dc}. They analyzed the stability of fixed points by a linearizing technique [39] and clarified the conditions under which bifurcations appear between the switching

*nozaki@phys.keio.ac.jp

phases, which consist of different numbers of fixed points, saddle points, and limit cycles. They identified the critical H_{ac} in MAS as the intersection of two bifurcations, namely, a saddle-node bifurcation and Andronov-Hopf bifurcation. However, this analytical technique for studying nonlinear MAS dynamics is applicable only to systems that obey the macrospin model. In practical systems such as ECC media (whose dynamics cannot be fully described by the macrospin model), we must explore the conditions that induce bifurcations and the corresponding metastable states of the magnetization dynamics. Most of the conventional MAS studies have focused on the conditions of successful deterministic switching under an applied H_{ac}, which is unsuitable for exploring the bifurcations and metastable states of nonlinear magnetization dynamics. Moreover, to distinguish whether the nonlinearly excited magnetization precession aids or suppresses MAS, we should quantify the effective potential barrier height ΔU^{eff}. However, whereas the amplitude of the magnetization precession angle can be measured by its magneto-optical or magnetoresistance effect, few experimental techniques are available for measuring the ΔU^{eff}.

Recently, we developed a cooperative switching (CS) method [40] for measuring ΔU^{eff} and demonstrated the oscillatory variation of ΔU^{eff} during transient magnetization precession in NiFe strips excited by a strong H_{ac} [41]. Applying the CS method, we here demonstrate a nontrivial variation of ΔU^{eff} for magnetization switching in sub-μm-wide ferromagnetic NiFe strips. The CS method semiquantitatively measures the ΔU^{eff} at a given point in the nonequilibrium state of magnetization precession using a sub-ns-wide orthogonal field impulse. Comparing the experimental results and micromagnetic calculations, we attributed the ΔU^{eff} changes under a negative H_{dc} to a saddle-node bifurcation, as predicted by the macrospin model. At the uniform growth stage of the precession, the saddle-node bifurcation appeared, although after sufficient growth nonlinear magnon scattering subsequently occurred and formed standing spin waves.

The remainder of this paper is organized as follows. Section II briefly analyzes the nonlinear dynamics under a strong H_{ac} in the macrospin model. This analysis highlights the switching phases and the bifurcations remarked on in the paper. The experimental setup of the CS method and the principle of evaluating ΔU^{eff} by CS are described in Sec. III. The experimental ΔU^{eff} results of the metastable MAS states are given in Sec. IV. Section V describes the numerical simulation results of CS and discusses the nonlinear dynamics of MAS below the critical amplitude of H_{ac} by comparing the experimental and numerical results. The paper concludes with Sec. VI.

II. ANALYTICAL STUDY ON NONLINEAR DYNAMICS IN MAS

This section briefly introduces the nonlinear dynamics of MAS, which were theoretically analyzed by Bertotti *et al*. The magnetization dynamics are governed by the Landau-Lifshitz-Gilbert (LLG) equation in normalized form:

$$\frac{d\boldsymbol{m}}{dt} = -\boldsymbol{m} \times \boldsymbol{h}_{\text{eff}} + \alpha \boldsymbol{m} \times \frac{d\boldsymbol{m}}{dt}, \tag{1}$$

where $\boldsymbol{m}$ is the unit vector of local magnetization and α is the Gilbert damping coefficient. $\boldsymbol{h}_{\text{eff}}$ is the reduced effective field consisting of $\boldsymbol{h}_{ac} = \boldsymbol{H}_{ac}/M_s$, $\boldsymbol{h}_{dc} = \boldsymbol{H}_{dc}/M_s$, and a uniaxial anisotropy field $\boldsymbol{h}_{\text{uni}}$. Here time is measured in units of γM_s where γ is the gyromagnetic ratio. The nonlinear magnetization dynamics induced by H_{ac} can be simplified in a rotating reference frame synchronized with H_{ac}. In the rotating coordinate system, Eq. (1) becomes

$$\frac{d\boldsymbol{m}}{dt} = -\boldsymbol{m} \times [\boldsymbol{h}_{\text{eff}} - \boldsymbol{\omega} + \alpha \boldsymbol{m} \times \boldsymbol{\omega}] + \alpha \boldsymbol{m} \times \frac{d\boldsymbol{m}}{dt}. \tag{2}$$

In the rotating frame, an additional inertial magnetic field $\boldsymbol{\omega}$ appears and $\boldsymbol{h}_{dc}$, $\boldsymbol{h}_{ac}$, $\boldsymbol{h}_{\text{uni}}$, and $-\boldsymbol{\omega}$ are all static. As shown in Eq. (2), the magnetic torques are always orthogonal to $\boldsymbol{m}$ and the amplitude of the magnetization vector $\boldsymbol{m}$ is temporally invariant. Consequently, the temporal evolution of the magnetization vector is restricted to the surface of a unit sphere and its dynamics can be expressed in (θ, ϕ) polar coordinates by substituting $\boldsymbol{m} =(\sin\theta\cos\phi, -\sin\theta\sin\phi, \cos\theta)$. Finally, the LLG equation can be expressed as follows:

$$\frac{d\theta}{dt} - \alpha \sin\theta \frac{d\phi}{dt} = h_{ac} \sin\phi - \alpha\omega \sin\theta, \tag{3}$$

$$\alpha \frac{d\theta}{dt} + \sin\theta \frac{d\phi}{dt} = h_{ac} \cos\phi \cos\theta - (h_{dc} - \omega + h_{\text{uni}} \cos\theta) \sin\theta. \tag{4}$$

Although the dynamical system represented by Eqs. (3) and (4) is highly nonlinear and too complex to solve analytically, stationary solutions (θ_0, ϕ_0) can be obtained by setting the time derivative terms to zero. These stationary solutions can be categorized based on their stability against perturbations. Here, we represent a perturbation by the infinitesimal displacement $(\Delta\theta, \Delta\phi)$ and substitute (θ, ϕ) in Eqs. (3) and (4) by the perturbed coordinate $(\theta_0 + \Delta\theta, \phi_0 + \Delta\phi)$. Then, the linearized equation for the displacement can be obtained as

$$\frac{d}{dt}\begin{bmatrix}\Delta\theta \\ \Delta\phi\end{bmatrix} = A_0 \begin{bmatrix}\Delta\theta \\ \Delta\phi\end{bmatrix}, \tag{5}$$

$$A_0 = \frac{1}{1+\alpha^2}\begin{bmatrix}1 & -\alpha \\ \alpha & 1\end{bmatrix}\begin{bmatrix}-\alpha\omega\cos\theta_0 & \nu_0 \\ \nu_0 - h_{\text{uni}}\sin^2\theta_0 & -\alpha\omega\cos\theta_0\end{bmatrix} \tag{6}$$

with

$$\nu_0 = \alpha\omega\cos\phi_0. \tag{7}$$

It is particularly known that a linearized equation with two valuables, such as $\frac{d}{dt}\boldsymbol{x}' = A'\boldsymbol{x}'$, has a supercomposed solution, $\boldsymbol{x}'(t) = c_1 e^{\lambda_1 t}\boldsymbol{v}_1 + c_2 e^{\lambda_2 t}\boldsymbol{v}_2$, where A' is a 2×2 real matrix, $\boldsymbol{x}'$ is two-dimensional vector field, $\lambda_{1(2)}$ is the eigenvalue for eigenvector $\boldsymbol{v}_{1(2)}$, respectively. The eigenvalue of Eq. (5) is given by

$$\lambda_{1(2)} = \frac{\text{tr}A_0 \pm \sqrt{(\text{tr}A_0)^2 - 4\det A_0}}{2}. \tag{8}$$

The combination of the signs of λ_1 and λ_2 determines the stability of the corresponding fixed points (θ_0, ϕ_0). The fixed points are saddle points when $\det A_0 < 0$ and node (or focus) points when $\det A_0 > 0$. A node or focus is stable if $\text{tr}A_0 > 0$ and unstable if $\text{tr}A_0 < 0$. The expressions $\text{tr}A_0 = 0$ and $\det A_0 = 0$ define the boundaries of the dynamical states defined by the number and stability of the fixed points.

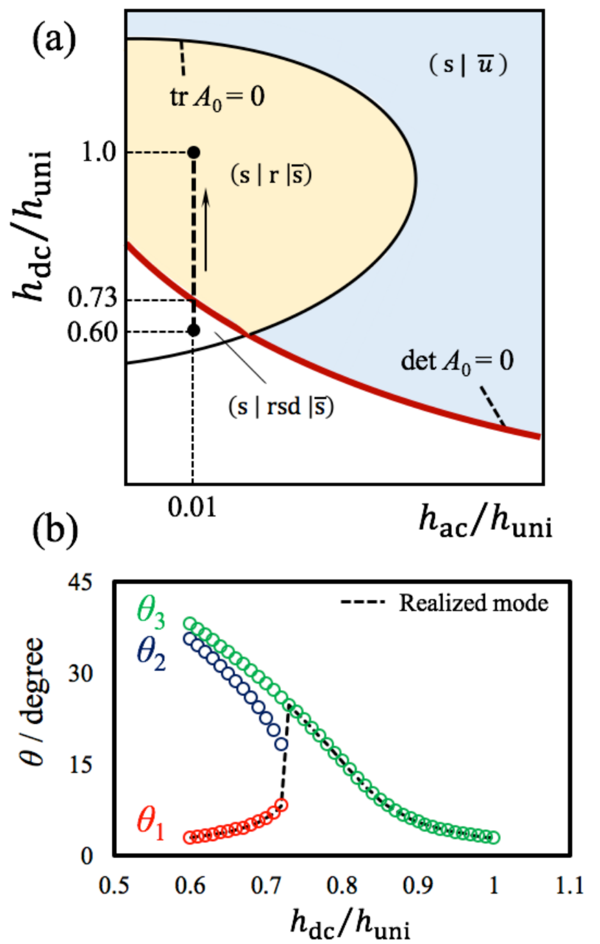

FIG. 1. (a) Schematic of the phase diagram reported by Bertotti *et al.* [32]. The lines of $\mathrm{tr}A_0 = 0$ and $\det A_0 = 0$ correspond to the saddle-node and the Andronov-Hopf bifurcation, respectively. The labels s, u, and d denote the existence regions of stable, unstable, and saddle-type fixed points. The fixed points number 2 or 4. The bars above the labels indicate the initial state. (b) Cylindrical coordinate θ of the fixed points calculated along the dashed line in (a). Although four fixed points exist in the $(s|rsd|\bar{s})$ region, two of them disappear across the $\det A_0$ line.

Figure 1(a) shows the phase diagram of MAS plotted in the control plane (h_{ac},h_{dc}). This phase diagram was given by Bertotti *et al.* [32], for a system with uniaxial anisotropy subject to a circularly polarized microwave field. The characters s, u, and d in Fig. 1(a) denote the existence of stable, unstable, and saddle-type fixed points in the phase portrait, respectively. Besides the fixed points, the phase space admits self-oscillatory steady states called limit cycles, which frequently appear in nonlinear systems. In Fig. 1(a), the character r denotes a repelling limit cycle. The other type of limit cycle (i.e., the attracting cycle) plays an important role in realizing magnetization auto-oscillations in a spin-torque oscillator, which generates a circularly polarized magnetic field in MAMR. However, to obtain deterministic MAS, the limit cycle should be eliminated from the phase portrait.

To quantitatively understand the bifurcation, we calculated the change in the precession angle θ along the pathway indicated by the thick broken line in Fig. 1(a). Figure 1(b) shows the stationary solutions of θ obtained by solving Eqs. (3) and (4) with $d\theta/dt = d\phi/dt = 0$. Two stable fixed points (θ_1 and θ_3) and a stable saddle point (θ_2) appear when h_{dc}/h_{uni} is less than 0.73, but only θ_3 remains when h_{dc}/h_{uni} exceeds 0.73. Another stable fixed point appears in the southern hemisphere (i.e., $\theta > \frac{\pi}{2}$) of the phase portrait. Suppose that a magnetization vector initially oriented at $\theta = 0$ is simultaneously subjected to $h_{ac}/h_{uni} = 0.01$ and $h_{dc}/h_{uni} < 0.73$. In this case, the precession angle is relaxed at θ_1, the nearest fixed point from the initial direction. As h_{dc}/h_{uni} increases, a pair annihilation of s and d (i.e., θ_1 and θ_2) becomes evident at $h_{dc}/h_{uni} = 0.73$ [Fig. 1(b)]. Qualitatively, this change is categorized as a saddle-node bifurcation. Consequent to the saddle-node bifurcation, the precession angle rapidly increases from θ_1 to θ_3 at $h_{dc}/h_{uni} = 0.73$. Therefore, the saddle-node bifurcation should manifest as a rapid change in the precession angle or a corresponding decrease of ΔU^{eff} in the switching phase diagram of MAS. In our experiments, we apply this principle to explore the saddle-node bifurcation in NiFe strips with lateral size above the applicable range of the macrospin approximation.

In the case of NiFe strip studied in our experiment, the anisotropy field in $\boldsymbol{h}_{\mathrm{eff}}$ is not associated with the cubic anisotropy but the shape anisotropy of the strip which leads to an asymmetry precession of magnetization. In other words, although the above analytical discussion is helpful to understand the principle of our experiment for exploring the saddle-node bifurcation, the analytical study given above is simple enough to completely describe the switching phase diagram of the NiFe strip.

III. EXPERIMENTAL METHOD

In Sec. III A, we briefly introduce the principle of the CS method for evaluating the instantaneous ΔU^{eff} after applying H_{dc} and H_{ac} simultaneously. Section III B presents the sample configuration and experimental setup.

A. Cooperative switching method

This section develops the principle of the CS method and demonstrates it on a ferromagnet with uniaxial anisotropy. Figure 2(a) illustrates the precession of magnetization excited by H_{ac} in the experimental coordinate system, where H_{dc} is held constant. Figure 2(b) plots the potential energy of the ferromagnet as a function of polar angle θ under negative H_{dc}. The H_{dc} resolves the Zeeman splitting degeneracy; subsequently, the initial state with $\theta = 0$ becomes metastable. When the frequency of the H_{ac} (which excites the ferromagnet) reaches the ferromagnetic resonance (FMR) frequency f_{FMR}, the ΔU^{eff} reduces [dashed orbit in Fig. 2(b)]. The magnetization reverses only when ΔU^{eff} becomes zero, implying that magnetization switching is prohibited when ΔU^{eff} remains finite. This situation is depicted in the $(s|r|\bar{s})$ region of Fig. 1(a). Conventional studies of MAS evaluate only whether magnetization switching occurs under the H_{ac} field, which is unlikely to reveal the shallow magnetic potential in the metastable state.

The CS method evaluates the ΔU^{eff} under simultaneous applications of H_{ac}, H_{dc} and a 100-ps-wide field impulse H_{pulse}. It should be noted that the H_{pulse} in the CS method

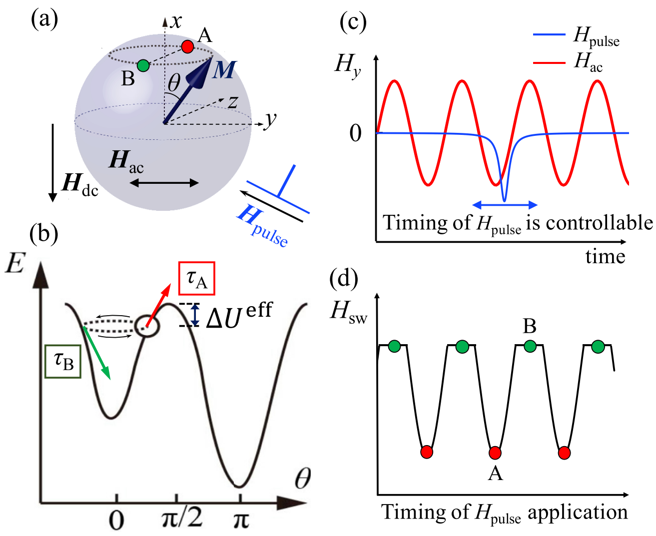

FIG. 2. Principle of the CS method. (a) Magnetization precession under the application of H_{ac} (|| y axis) and H_{dc} (|| x axis). θ denotes the angle between the magnetization and its favored axis. (b) Potential barrier under H_{dc} and H_{ac}. The initial state ($\theta = 0$) becomes metastable, but the magnetization switching is disturbed by the finite potential barrier ΔU^{eff}. τ_a and τ_b are the torques imparted by H_{pulse} when the magnetization vector is A and B in (a), respectively. (c) H_y components of H_{ac} (red) and H_{pulse} (blue). The application timing of H_{pulse} relative to H_{ac} is controllable. (d) Simplistic picture of the switching field vs application timing of H_{pulse}. At the best timing of H_{pulse} [namely, at the timing of A in (a) or (b)], the switching field decreases.

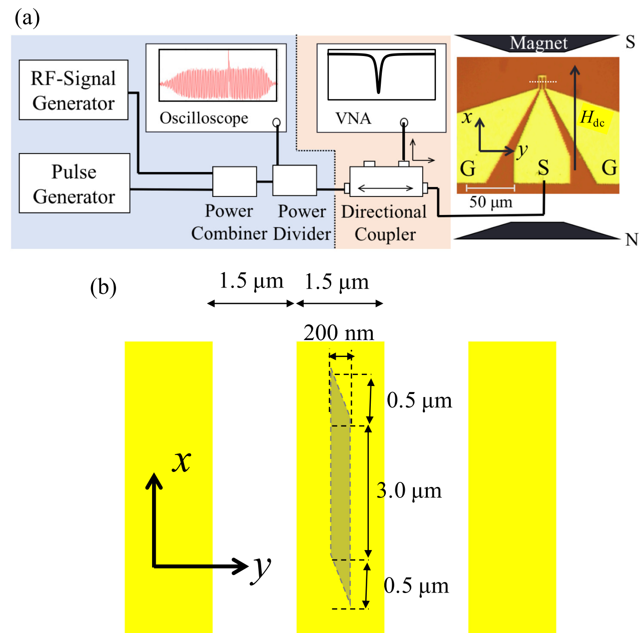

FIG. 3. (a) Setup of the cooperative switching experiment and a photomicrograph of our sample. The rf-signal generator generates a microwave impulse, and the pulse generator generates a 100-ps-wide pulsed current. Both currents are combined by the power combiner. The combined current is then divided by a power divider. As the combined current is applied to the coplanar waveguide (CPW), its divided wave forms are observed on an oscilloscope. The vector network analyzer (VNA) measures the ferromagnetic resonance spectra. (b) Enlarged view of the sample, showing its dimensions. The CPW and the NiFe strip are separated by a SiO_2 insulating layer.

is ten times shorter than the relaxation time of magnetization, which is approximated by $1/\alpha\omega$. The LLG equation [Eq. (1)] describes two kinds of magnetic torques with different temporal variations: a precessional motion torque with sub-ns variation and a damping torque that varies over a few nanoseconds. Thus, the short H_{pulse} applied in the CS method does not change the magnitude of the potential energy, but modulates the potential-energy profile in the phase space. Consequently, the trajectory of the magnetization precession is asymmetric about the z axis (the original precession axis), and the ΔU^{eff} changes over time. When the amplitude of H_{pulse} exceeds a threshold amplitude (which is proportional to the original ΔU^{eff} just before applying H_{pulse}), magnetization switching occurs. For this reason, the H_{pulse} can be used to evaluate ΔU^{eff} in the metastable state of the phase diagram in Fig. 1. The phase difference between H_{ac} and H_{pulse} is also significant in the CS method, because the magnetization precession and H_{ac} vary over the same time scale (GHz). Suppose that H_{pulse} is applied along the $-y$ direction in Fig. 2(a). Figure 2(c) shows the temporal development of the y components of H_{ac} and H_{pulse}. Figure 2(d) shows the switching field as a function of H_{pulse} application timing, which can be tuned in the CS method. When the magnetization directs toward A in Fig. 2(a), the magnetic torque induced by H_{pulse} increases θ [Fig. 2(b)]. Consequently, the H_{pulse} application decreases the switching field [see Fig. 2(d)]. On the contrary, when the magnetization directs toward B in Fig. 2(a), the magnetic torque induced by H_{pulse} suppresses θ [Fig. 2(b)]. In this case, the H_{pulse} exerts no effect on the switching field. Consequently, as schematized in Fig. 2(d), the switching field in the CS method periodically responds to the timing of the H_{pulse} application. Unfortunately, the relative timing of the H_{pulse} application is disturbed by timing jitter (±50 ps) in the microwave synthesizer generating the H_{pulse}. However, by averaging the switching fields of multiple CS measurements under a given experimental condition, we can evaluate the instantaneous value of ΔU^{eff}.

B. Experimental setup

Figures 3(a) and 3(b) show the overall experimental setup of the CS and the sample dimensions. All samples were fabricated by electron-beam lithography, Ar^+ sputtering and electron-beam evaporation. A NiFe strip of thickness 35 nm, width 200 nm, and length 4 μm was deposited on a Si substrate. Next, a 100-nm-thick insulating SiO_2 and a coplanar waveguide (CPW) composed of Au (120 nm)/Ti (5 nm) were deposited. The signal line of the CPW was 1.5 μm wide and 10 μm long and was spaced 1.5 μm from the ground plane. A 25-ns-wide microwave impulse and a 100-ps-wide rectangular impulse were supplied by a signal generator (Anritsu MG3694B) and a pulse generator (Picosecond PSPL 10060), respectively. These signals were combined by a power combiner and applied to the CPW. The combined signal provided the in-plane H_{ac} and H_{pulse} applications along the width of the NiFe strip. Note that the phase difference between H_{ac} and H_{pulse} can be observed on an oscilloscope. The external magnetic field H_{dc} was always applied along the x axis. The CPW was also connected to a vector network analyzer (VNA: Agilent E8363C) via a broadband directional coupler [Fig. 3(a)]. A frequency-domain FMR spectrum of the NiFe strip can be obtained by measuring the microwave reflection coefficient, S_{11}, as a function of microwave frequency.

To demonstrate the CS, the NiFe strip was first magnetically saturated in the $-x$ direction by setting $H_{dc} = -1$ kOe. Second, a positive magnetic field H_{dc} with weaker amplitude than the coercive field was applied. To verify whether H_{ac} and H_{pulse} assisted the magnetization reversal, the combined microwave signal was applied to the CPW at the H_{dc}. After terminating the microwave signal, the f_{FMR} of the NiFe strips was measured by VNA ferromagnetic resonance spectroscopy. This measurement sequence was repeated while increasing H_{dc} to 360 Oe at +4 Oe intervals. The switching field of the NiFe strip manifested as discontinuous increases in f_{FMR}. The estimation of a switching field from f_{FMR} behavior is described in [4].

IV. EXPERIMENTAL RESULTS

This section presents the results of three experiments. Experiment (A) determines the magnetic and FMR properties of the NiFe strips, experiment (B) is an ordinary MAS experiment without the H_{pulse} application, and experiment (C) is the CS experiment applying both H_{ac} and H_{pulse}.

A. FMR properties

Magnetization switching was detected from the change in f_{FMR}. The inset of Fig. 4 shows the frequency dependence of the S_{11} parameter measured at $H_{dc} = 240$ Oe. The microwave absorbed by the FMR is clearly observed at 7.3 GHz. The value of f_{FMR} is defined as the absorption dip. Figure 4 plots the f_{FMR} as a function of the external field H_{dc}. f_{FMR} gradually decreased with increasing H_{dc} until H_{dc} reached 328 Oe. Note that f_{FMR} suddenly increased from 6.2 to 9.2 GHz at $H_{dc} = 332$ Oe and then monotonously increased with further increase of H_{dc}. The discontinuity in f_{FMR} is attributed to reversal of the relative orientation of the magnetization from antiparallel to parallel with respect to H_{dc}. Thus, the H_{dc} at which f_{FMR} becomes discontinuous can be regarded as the switching field of the NiFe strip. In this experiment, the static switching field of the strip appeared at 332 Oe (Fig. 4). In the following subsections, the switching fields of MAS in NiFe strips are presented under various conditions of the assistant field.

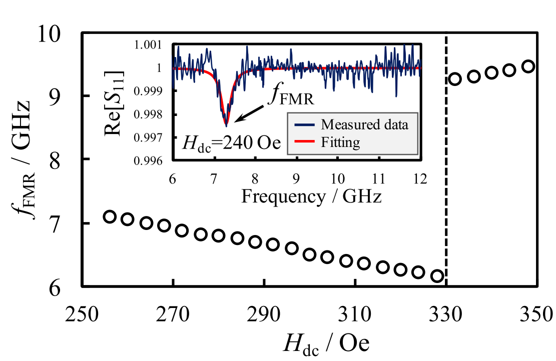

FIG. 4. External field dependence of the f_{FMR}. f_{FMR} decreases as H_{dc} is swept up to 332 Oe. At 332 Oe, the f_{FMR} suddenly jumps and increases linearly thereafter. Inset: Ferromagnetic resonance spectrum measured by the VNA at $H_{dc} = 240$ Oe.

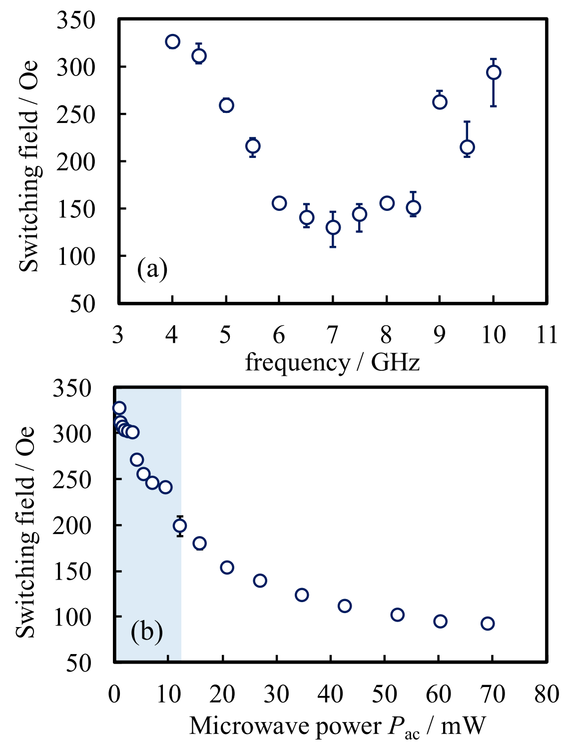

FIG. 5. (a) Switching field as a function of microwave frequency. The microwave power was fixed at 5.5 mW. The switching field is minimized at $f_{FMR} = 7.0$ GHz, providing clear evidence of MAS. (b) Switching field as a function of microwave power P_{ac} at fixed microwave frequency (5.0 GHz). The decrease is discontinuous at 5.5 and 12.1 mW.

B. Switching with an assistance of the microwave impulse alone

Before showing the results of the CS experiment, we examine MAS switching field without H_{pulse}. Figure 5(a) shows the microwave-frequency dependence of the switching fields. Here, the power of the microwave impulse was fixed at 5.5 mW. The switching field was minimized around 7.0 GHz, consistent with the f_{FMR} immediately before switching (Fig. 4). This indicates that the switching field in Fig. 5(a) is caused by FMR excitation.

Figure 5(b) plots the switching field as a function of microwave power P_{ac}, with the microwave frequency fixed at 5.0 GHz. The switching field decreased with P_{ac} but rapidly decreased at $P_{ac} = 5.5$ and 12.1 mW. In the simple analysis of MAS using the macrospin model, the switching field exhibits a similar discontinuous change at the critical amplitude of H_{ac} [the field at which the discontinuity appears is marked by the intersection of the tr$A_0 = 0$ and det$A_0 = 0$ lines in Fig. 1(a)]. In the $(s|u)$ state in Fig. 1(a), the magnetization switching is deterministic because the initial magnetization state becomes unstable and a stable fixed point exists only in the southern hemisphere. When H_{ac} exceeds the critical value, the $(s|u)$

state can be realized after the saddle-node bifurcation given by $\det A_0 = 0$. On the contrary, when H_{ac} is below the critical value, the stable fixed point in the northern hemisphere does not disappear even if the saddle-node bifurcation takes place [Fig. 1(a)]. To obtain the $(s|u)$ state needed for the deterministic reversal of magnetization, the Andronov-Hopf bifurcation (given by $\mathrm{tr} A_0 = 0$) should take place. In the Andronov-Hopf bifurcation, the fixed point in the northern hemisphere becomes unstable and the repelling limit cycle disappears. To achieve the Andronov-Hopf bifurcation, H_{dc} must be larger than H_{dc} at the saddle-node bifurcation. Therefore, the discontinuous change in the switching field arises from the different bifurcations required for deterministic switching. When the metastable state disappears, the switching field suddenly decreases. Thus, the discontinuous changes in the switching field observed in the NiFe strip imply that a metastable state exists below the H_{ac}, at which the switching field discontinuously decreases. In other words, the expected saddle-node bifurcation of the metastable state below the critical H_{ac}, i.e., the bifurcation from $(s|rsd|\bar{s})$ to $(s|r|\bar{s})$ in Fig. 1(a), will appear in the hatched region of Fig. 5(b). The appearance of two discontinuous changes, rather than the single discontinuity predicted by the macrospin model, is not understood but is possibly attributable to the nonuniform MAS in the NiFe strip. Moreover, the phase diagram predicted by the macrospin model is applicable only when the magnetization dynamics start from stationary states, namely, θ_1 or θ_3 in Fig. 1(b), with no thermal fluctuations. In practical systems at finite temperature, an initial state with $\theta = 0$ is more energetic than the nearest fixed point [34]. Therefore, not only the thermal energy but also the initial energy can transcend the barrier related to the repelling limit cycle between two stable fixed points. Consequently, the switching field can decrease from the value that induces the Andronov-Hopf bifurcation.

C. Cooperative switching experiment

Finally we demonstrate the CS in the NiFe strip, with simultaneous application of H_{ac} and a 100-ps-wide H_{pulse}. A representative combined wave form is shown in Figs. 7(a) and 7(b). The frequency and power of H_{ac} were fixed at 5.0 GHz and 5.5 mW, respectively. The time difference between the beginnings of the H_{ac} and H_{pulse} applications was fixed at 15 ns throughout the experiments. The relaxation time ($\tau_{relax} = \frac{1}{2\pi f_{FMR}\alpha}$) of the NiFe strip (a few ns) was approximately estimated from the f_{FMR} before switching, which ranged from 6.0 to 8.0 GHz. Therefore, the magnetization dynamics reached steady state before the H_{pulse} application. Figure 6 shows histograms of the switching field distribution under various magnitudes of H_{pulse}: 95 Oe (a), 150 Oe (b), and 200 Oe (c). The experiments were carried out 80 times in Fig. 6(b) and 20 times in Figs. 6(a) and 6(c). The CS requires plural experiments to average the influence of the timing jitter in the H_{pulse} generator. Because the H_{pulse} duration (100 ps) is shorter than the period of H_{ac} (200 ps), the phase difference between H_{ac} and H_{pulse} determines whether a switch occurs or not. The H_{pulse} application timing was randomly varied within the 50-ps timing jitter, causing fluctuations in the CS field. It should be noted that if the CS occurs, the scattering of the switching fields is distributed below

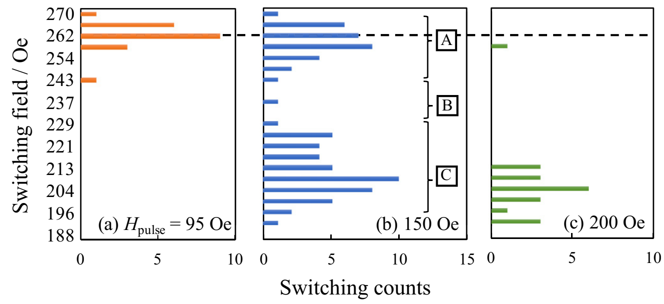

FIG. 6. Switching field distributions at H_{pulse} strengths of (a) 95 Oe, (b) 150 Oe, and (c) 200 Oe. The CS experiment was iterated 20 times in (a) and (c) and 80 times in (b). Dashed line in each panel indicates the switching field under H_{ac} alone. The switching field does not decrease monotonously with H_{pulse}. In (b), there are many switches in regions A and C and few switching events in region B.

the switching field measured without the H_{pulse} application [Fig. 2(d)]. The H_{dc} strength was increased from 0 to 360 Oe at 4-Oe intervals. As mentioned above, H_{pulse} was set to 95, 150, or 200 Oe. When the magnetization reversed, the count number of the corresponding switching field was increased by 1 and the increase of H_{dc} was terminated. After initializing the magnetization of the NiFe strip by $H_{dc} = -1$ kOe, the H_{dc} was increased stepwise and simultaneously applied with H_{pulse} until the switching recurred. The lowest-strength H_{pulse} (95 Oe) provided little assistance to the CS field. The switching field was scattered around 262 Oe, which coincides with the switching field induced by H_{ac} alone (applied at 5.0 GHz and 5.5 mW). In this case, the aid provided by the H_{pulse} application could not sufficiently decrease the effective barrier to induce magnetization reversal. At 200 Oe, the H_{pulse} application clearly decreased the switching field [Fig. 6(c)]. Specifically, the scattering center of the switching field decreased from 262 to 204 Oe. If the H_{pulse} application suppresses the switching field proportionally to the amplitude of H_{pulse}, the scattering center of the switching field will monotonously decrease. However, under an intermediate-strength H_{pulse} (150 Oe), the scattering of the switching fields appeared in two distinct H_{dc} zones [around 204 and 262 Oe; Fig. 6(b)]. The magnetization reversal was sparse in the 230–240-Oe range. This result cannot be explained by the Zeeman effect, where increasing an H_{dc} field that opposes the magnetization monotonously decreases the ΔU^{eff}. Such a nontrivial switching is attributed to the nonlinear dynamics of MAS. When describing the principle of the CS method, we mentioned that ΔU^{eff} at a given H_{dc} can be estimated just before applying H_{pulse}. Therefore, Fig. 6(b) implies that ΔU^{eff} ($H_{dc} = 204$ Oe) is lower than ΔU^{eff} ($H_{dc} = 237$ Oe), although the Zeeman energy decreases less in the former than in the latter case. This nontrivial variation in ΔU^{eff} with respect to H_{dc} was confirmed in a micromagnetics simulation of the CS in the NiFe strip. Note that when H_{pulse} exceeded 200 Oe, the switching field no longer decreased. This result indicates that ΔU^{eff} changes rapidly, not slowly, from $H_{dc} = 204$ Oe. Our micromagnetics simulation supports this expectation (see Sec. V).

To confirm that the separated scattering of the switching field is not caused by timing-jitter fluctuations in the switching field, we checked the combined wave form of $H_{ac} + H_{pulse}$ in

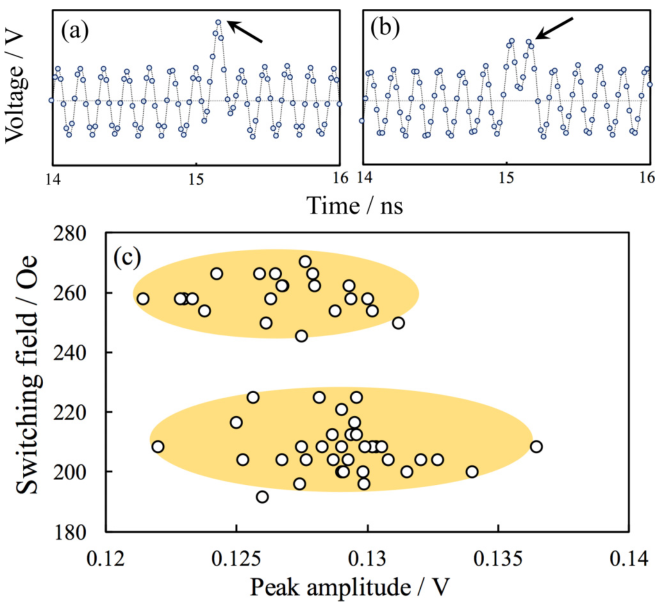

FIG. 7. Influence of timing jitter on the switching field scattering in the CS experiment: (a) and (b) Examples of the combined wave forms measured by the oscilloscope. The arrow in (a) and (b) points to the peak amplitude. (c) Scattering plots of the switching field with respect to the peak amplitude. The two factors are uncorrelated, indicating that the separation of the switching field scatter in Fig. 6(b) is not caused by jitter.

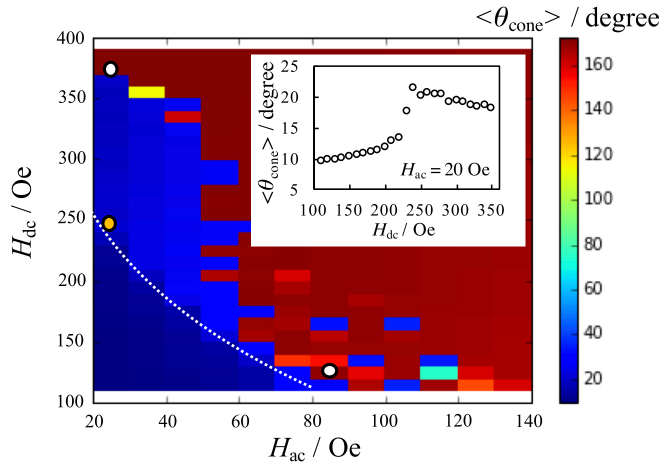

FIG. 8. Results of the micromagnetics simulation. Color plot of the time-averaged precession angle $\langle\theta_{\mathrm{cone}}\rangle$. The microwave frequency was 5.0 GHz and $\langle\theta_{\mathrm{cone}}\rangle$ was averaged between 5 and 6 ns. Switching is absent in the blue regions and observed in the red regions. A wide metastable region appears when $H_{\mathrm{ac}} < 60$ Oe. Furthermore, $\langle\theta_{\mathrm{cone}}\rangle$ increases suddenly across the white dashed line. This tendency is clarified by clipping the data at $H_{\mathrm{ac}} = 20$ Oe (inset). After a sudden increase, $\langle\theta_{\mathrm{cone}}\rangle$ is locally maximized at $H_{\mathrm{dc}} = 240$ Oe.

each CS experiment. Figures 7(a) and 7(b) show examples of combined wave forms with different timing jitters. In Fig. 7(a), the maxima of the superimposed H_{pulse} matches those of H_{ac}. When the timing of the H_{pulse} application is shifted from the perfectly matched case, the peak intensity of the combined wave form decreases [indicated by the arrow in Fig. 7(b)]. Figure 7(c) is a scattering plot of the switching field with respect to the peak intensity of the combined wave forms. The scattering clearly separates into two regions, although the peak intensity of the combined wave form is monotonously scattered. We conclude that the separation of the switching field scattering is not caused by the undesirable deviation of the timing jitter.

V. MICROMAGNETICS SIMULATION

To understand the nontrivial variation in ΔU^{eff} in Fig. 6, we simulated the micromagnetic dynamics in MuMax3 [42]. The saturation magnetization, exchange stiffness constant, and Gilbert damping coefficient were set to $4\pi M_s = 10$ kG, $A_{\mathrm{ex}} = 1.3 \times 10^6$ erg/cm, and $\alpha = 0.01$, respectively. Thermal agitation at 300 K was assumed. The sample geometry was identical to the experimental setup. The numerical grid was sized $5 \times 5 \times 5$ nm^3, where each side is comparable to the exchange length l_{ex} of NiFe (5.7 nm) [24].

A. Magnetization dynamics under H_{ac} alone

First, the magnetization dynamics were calculated under the H_{ac} application. The rise time and frequency of H_{ac} were set to zero and 5.0 GHz, respectively. The magnetization dynamics were evolved over 6 ns. The relaxation time τ_{relax} of the NiFe strips was calculated as $\tau_{\mathrm{relax}} = 3.2$ ns. Consequently, the time-averaged precession angle $\langle\theta_{\mathrm{cone}}\rangle$, needed for evaluating the amplitude of the magnetization excitation in the NiFe strip, was 5–6 ns. $\langle\theta_{\mathrm{cone}}\rangle$ was also averaged over the entire sample. Figure 8 is a color plot of $\langle\theta_{\mathrm{cone}}\rangle$ at $f_{\mathrm{ac}} = 5.0$ GHz versus H_{ac} and H_{dc}. The magnetization switching requires larger H_{dc} when $H_{\mathrm{ac}} < 60$ Oe than when $H_{\mathrm{ac}} > 60$ Oe, qualitatively consistent with the experimental results [see Fig. 5(b)]. The most notable aspect of the metastable (blue) region is the sudden increase of the precession angle $\langle\theta_{\mathrm{cone}}\rangle$ along the dashed white line. The inset in Fig. 8 plots $\langle\theta_{\mathrm{cone}}\rangle$ as a function of H_{dc} when $H_{\mathrm{ac}} = 20$ Oe. $\langle\theta_{\mathrm{cone}}\rangle$ began increasing at $H_{\mathrm{dc}} = 230$ Oe, reached its local maximum at $H_{\mathrm{dc}} = 240$ Oe, and then gradually decreased. The inset in Fig. 8 shows that in the metastable region, $\langle\theta_{\mathrm{cone}}\rangle$ reaches a maximum of 23°: this is similar to the analytical results [Fig. 1(b)] when a large angle precession with 22° is realized at the saddle-node bifurcation. Suto *et al.* also numerically showed that a precession with an angle as large as 30° appears in the $(s|r|\bar{s})$ region [34]. Moreover, it was experimentally confirmed that the amplitude of the precession angle in the Co/Ni multilayer measured using the magneto-optical Kerr effect reached 20° when a foldover effect was observed for strong excitation [43]. The sudden increase in $\langle\theta_{\mathrm{cone}}\rangle$ in the metastable state is attributed to the saddle-node bifurcation, as similarly seen in the macrospin model. The numerical result suggests that ΔU^{eff} is locally minimized in the metastable states of the switching phase diagram. This might explain the separated switching field scattering observed in Fig. 6(b). However, because ΔU^{eff} also depends on the pathway of magnetization reversal in the contour map of the potential energy, it is not always reduced by increasing the $\langle\theta_{\mathrm{cone}}\rangle$. Therefore, to confirm the existence of the local minimum of ΔU^{eff} in the metastable state, we must

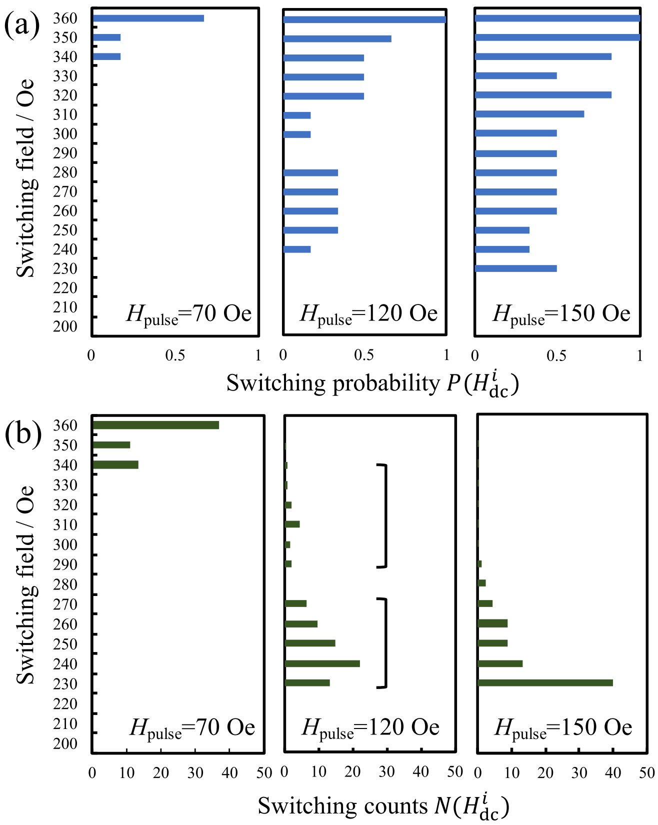

FIG. 9. Results of the micromagnetics simulation. H_{dc} dependence of (a) the switching probability $P(H_{dc})$ and (b) the switching field distribution $N(H_{dc})$. In both sets of results, H_{pulse} was varied as 70, 120, and 150 Oe. The switching probability is bimodal at $H_{pulse} = 120$ Oe, as similarly observed in Fig. 6(b).

simulate the micromagnetics under the application of both H_{ac} and H_{pulse}.

B. Magnetization dynamics under the simultaneous application of H_{ac} and H_{pulse}

We then carried out the CS simulation. The amplitude and frequency of H_{ac} were unchanged from the previous calculation. The additional H_{pulse} was delayed by 7 ns from the beginning of the H_{ac} application. The phase difference ($\Delta\phi_{pulse}$) between H_{ac} and H_{pulse} plays an important role in switching in CS. To account for the influence of the timing jitter from the H_{pulse} generator, the CS micromagnetics were simulated at each H_{dc} strength with six timings of H_{pulse} application, i.e., 7 ns + $\frac{200\text{ns}}{6} \times n$ (for $n = 0,1,\ldots,5$). The switching probability $P(H_{dc})$ was obtained as the number of switching events at a given H_{dc}, divided by 6. The H_{dc} was varied from 200 to 360 Oe at 10-Oe intervals. Figure 9(a) shows the $P(H_{dc})$ for H_{pulse} amplitudes of 70, 120, and 150 Oe. As H_{pulse} increased, the range of H_{dc} with high switching probability was enlarged in the lower amplitude direction, although the switching probability also exhibited a fine structure. Note that at $H_{pulse} = 120$ Oe and $H_{dc} = 280$ Oe, the switching probability completely vanished despite the magnetization reversal occurring at H_{dc} amplitudes below 280 Oe. This provides clear evidence of a local ΔU^{eff} minimum in the metastable state. To confirm that the H_{dc} distribution of the switching probability underlies the separation of the switching field scattering [as experimentally observed in Fig. 6(b)], we simulated the experimental sequence using the switching probability data in Fig. 9(a). The expected number of switching events in successive CS experiments is given by

$$N(H^0_{dc}) = P(H^0_{dc}) \times N,$$
$$N(H^1_{dc}) = P(H^1_{dc}) \times [N - N(H^0_{dc})],$$
$$N(H^2_{dc}) = P(H^2_{dc}) \times \{N - [N(H^0_{dc}) + N(H^1_{dc})]\}$$
$$\cdots$$
$$N(H^i_{dc}) = P(H^i_{dc}) \times \left[N - \sum_{j\leqslant i-1} N(H^j_{dc}) \right], \tag{9}$$

where N is the total number of CS trials and H^i_{dc} is the ith external magnetic field accompanied by H_{pulse} in the CS simulation. To reproduce the experiment in Fig. 6, we set $N = 80$ and calculated the number of switched cases for each switching field. Figure 9(b) shows the calculated numbers of switching events as functions of H_{dc} for H_{pulse} amplitudes of 70, 120, and 150 Oe. When the H_{pulse} was 70 and 150 Oe, the scattering of the switching fields was concentrated in the field ranges 340–360 Oe and 230–280 Oe, respectively. In contrast, the 100-Oe H_{pulse} yielded a bimodal scattering of the switching fields, similar to the experimental results in Fig. 6(b). Therefore, we can confidently attribute the separation of the switching field scattering to the local minimization of ΔU^{eff} by the saddle-node bifurcation in the metastable state. That is, the CS method can explore the bifurcation in the metastable state of the switching phase diagram.

C. Switching processes

Finally, we discuss the magnetization reversal process in MAS. Figures 10(a) and 10(b) show transient reversals of the magnetic domain configuration when $H_{ac} < H_{th}$ and $H_{ac} > H_{th}$, respectively, where H_{th} is the critical amplitude of H_{ac} for MAS induction. The numerical conditions are indicated by open circles in Fig. 8. When $H_{ac} < H_{th}$, the magnetization domains at the ends of the NiFe strip were reversed followed by domain-wall propagation. In contrast, under the conditions of successful MAS (i.e., $H_{ac} > H_{th}$), the precession angles coherently increased in the NiFe strip, and the magnetization was rotated into the reverse orientation throughout the whole body. Figure 10(c) shows transients of the magnetization configuration under the conditions of the saddle-node bifurcation $(H_{ac}, H_{dc}) = (20$ Oe, 270 Oe) (indicated by the yellow circle in Fig. 8). The magnetization precession increased uniformly over the first 4.00 ns. Thereafter, standing spinwave modes appeared along the longitudinal direction. One of the possible origins for generating the standing wave is a four-magnon scattering process where two magnons with zero wave vector k are scattered into two magnons with $k \neq 0$. It was noted that the scattered magnons had the same amplitude but had opposite signs, which generated standing spinwaves in the NiFe strip. A nonuniform excitation of spinwaves due to the lack of translational symmetry breaking at the edge of the NiFe strip also causes the standing spinwaves [44,45]. However, we

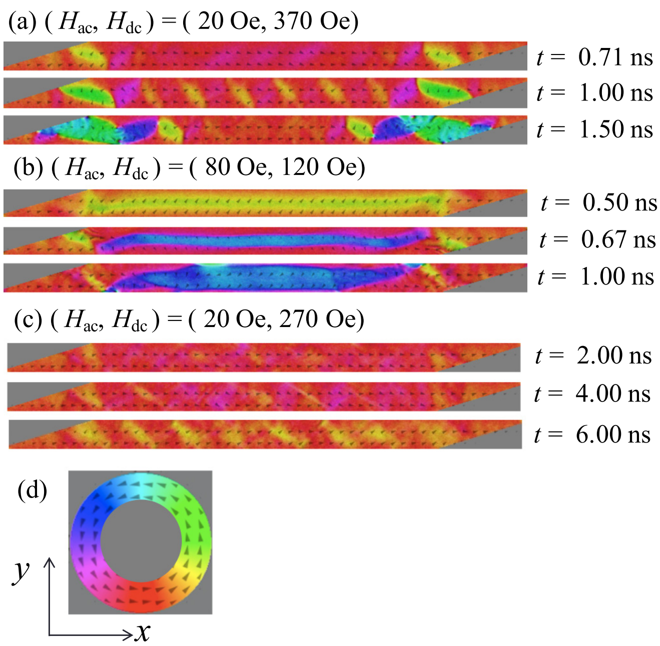

FIG. 10. Snapshots of the magnetization dynamics excited in the NiFe strip. Magnetization switching occurs when $(H_{ac}, H_{dc}) =$ (20 Oe, 370 Oe) in panel (a) and (80 Oe, 120 Oe) in panel (b). In (a), domains nucleate at both edges of the NiFe strip, whereas in (b), the magnetization switching is associated with coherent rotation. (c) Snapshots of the growing magnetization precession when $(H_{ac}, H_{dc}) = (20$ Oe, 270 Oe). In the initial process ($t =$ 0.00–4.00 ns), the precession increases uniformly, but after $t = 4.00$ ns the uniform mode evolves into a standing spin-wave mode. (d) Correspondence of the magnetization direction with the color map.

also confirmed that the formation of standing spin waves in Fig. 10 was independent of the edge geometry of the NiFe strip. The result suggests that the four magnon scattering is the main reason for the appearance of standing spin waves in the NiFe strip.

Even in the large ferromagnets that cannot be described by the macrospin model, successful MAS when $H_{ac} > H_{th}$ is associated with a uniform growth of a large angular rotation of the magnetization. When $H_{ac} < H_{th}$, the saddle-node bifurcation appeared, although the stationary states consisted of standing spin waves. In large ferromagnets, the deterministic switching was hindered not by a metastable uniform mode (i.e., a mode with a stable fixed point s in the macrospin model), but by the formation of spin waves. However, the switching phase diagram of MAS in large ferromagnets might be similar to that predicted by the macrospin model, because the four-magnon scattering process also requires the strong excitation of uniform magnons at the saddle-node bifurcation.

VI. CONCLUSION

In a CS experiment, we probed the instantaneous height of ΔU^{eff} by a 100-ps pulsed magnetic field and thereby investigated the properties of the nonlinearly excited magnetization dynamics in the metastable switching region. The experimental results revealed a nontrivial reduction of ΔU^{eff} in the metastable switching region. The behavior of ΔU^{eff} is consistent with the saddle-node bifurcation calculated by Bertotti *et al.* Our micromagnetics simulation not only reproduced the experimental results but also revealed uniform excitation at the start of the magnetization precession, and the standing spin waves formed by subsequent four magnon scattering. In large ferromagnets, deterministic switching was hindered by the formation of spin waves appearing after the saddle-node bifurcation. Even in large ferromagnets, the saddle-node bifurcation is significant to determine the critical condition for MAS. From the viewpoint of MAMR application, the CS can be a promising method to reduce the amplitude of H_{ac} required for a successful MAS because the application of very narrow H_{pulse} at a proper timing can help the MAMR even when H_{ac} is smaller than H_{th}.

ACKNOWLEDGMENTS

The authors thank Prof. Atsufumi Hirohata for valuable discussion and comments. This work was supported by the JSPS Core-to-Core program and JSPS KAKENHI Grant No. 26249052.

[1] A. H. Ferona and R. E. Camley, Phys. Rev. B **95**, 104421 (2017).
[2] C. Thirion, W. Wernsdorfer, and D. Mailly, Nat. Mater. **2**, 524 (2003).
[3] T. Moriyama, R. Cao, J. Q. Xiao, J. Lu, X. R. Wang, Q. Wen, and H. W. Zhang, Appl. Phys. Lett. **90**, 152503 (2007).
[4] Y. Nozaki, K. Tateishi, S. Taharazako, M. Ohta, S. Yoshimura, and K. Matsuyama, Appl. Phys. Lett. **91**, 122505 (2007).
[5] H. T. Nembach, H. Bauer, J. M. Shaw, M. L. Schneider, and T. J. Silva, Appl. Phys. Lett. **95**, 062506 (2009).
[6] Y. Nozaki, N. Narita, T. Tanaka, and K. Matsuyama, Appl. Phys. Lett. **95**, 082505 (2009).
[7] Y. P. Chen, X. Fan, Q. Lu, and J. Q. Xiao, J. Appl. Phys. **110**, 053905 (2011).
[8] S. Okamoto, N. Kikuchi, M. Furuta, O. Kitakami, and T. Shimatsu, Phys. Rev. Lett. **109**, 237209 (2012).
[9] S. Okamoto, N. Kikuchi, J. Li, O. Kitakami, T. Shimatsu, and H. Aoi, Appl. Phys. Express **5**, 043001 (2012).
[10] M Furuta, S. Okamoto, N. Kikuchi, O. Kitakami, and T. Shimatsu, Appl. Phys. Express **6**, 053006 (2013).
[11] N. Kikuchi, Y. Suyama, S. Okamoto, O. Kitakami, and T. Shimatsu, Appl. Phys. Lett. **104**, 112409 (2014).
[12] N. Kikuchi, M. Furuta, S. Okamoto, O. Kitakami, and T. Shimatsu, Appl. Phys. Lett. **105**, 242405 (2014).
[13] M Furuta, S. Okamoto, N. Kikuchi, O. Kitakami, and T. Shimatsu, J. Appl. Phys. **115**, 133914 (2014).
[14] Y. Nozaki, N. Ishida, Y. Soeno, and K. Sekiguchi, J. Appl. Phys. **112**, 083912 (2012).
[15] S. Okamoto, N. Kikuchi, A. Hotta, M. Furuta, O. Kitakami, and T. Shimatsu, Appl. Phys. Lett. **103**, 202405 (2013).
[16] N. Ishida, Y. Soeno, K. Sekiguchi, and Y. Nozaki, J. Appl. Phys. **114**, 043915 (2013).
[17] S. Okamoto, N. Kikuchi, O. Kitakami, and T. Shimatsu, Appl. Phys. Express **10**, 023004 (2017).
[18] Y. Nozaki and S. Kasai, IEEE Trans. Magn. **52**, 3100207 (2016).

[19] J. G. Zhu, X. Zhu, and Y. Tang, IEEE Trans. Magn. **44**, 1 (2008).
[20] J. G. Zhu, and Y. Wang, IEEE Trans. Magn. **46**, 3 (2010).
[21] S. Okamoto, N. Kikuchi, M. Furuta, O. Kitakami, and T. Shimatsu, J. Phys. D **48**, 353001 (2015).
[22] S. Okamoto, M. Igarashi, N. Kikuchi, and O. Kitakami, J. Appl. Phys. **107**, 123914 (2010).
[23] T. Taniguchi, Phys. Rev. B **90**, 024424 (2014).
[24] G. S. Abo, Y. K. Hong, J. Park, J. Lee, W. Lee, and B. C. Choi, IEEE Trans. Magn. **49**, 4937 (2013).
[25] S. Li, B. Livshitz, H. N. Bertram, M. Schabes, T. Schrefl, E. E. Fullerton, and V. Lomakin, Appl. Phys. Lett. **94**, 202509 (2009).
[26] S. Li, B. Livshitz, H. N. Bertram, E. E. Fullerton, and V. Lomakin, J. Appl. Phys. **105**, 07B909 (2009).
[27] T. Tanaka, A. Kato, Y. Furomoto, A. F. Md Nor, Y. Kanai, and K. Matsuyama, J. Appl. Phys. **111**, 07B711 (2012).
[28] J. Q. Goh, Z.-M. Yuan, L. Shen, T. Zhou, and Y. P. Feng, J. Appl. Phys. **111**, 066102 (2012).
[29] T. Tanaka, N. Narita, A. Kato, Y. Nozaki, Y. K. Hong, and K. Matsuyama, IEEE Trans. Magn. **49**, 562 (2013).
[30] T. Tanaka, S. Kashiwagi, Y. Otsuka, Y. Nozaki, Y.-K. Hong, and K. Matsuyama, IEEE Trans. Magn. **50**, 3000503 (2014).
[31] G. Bertotti, C. Serpico, and I. D. Mayergoyz, Phys. Rev. Lett. **86**, 724 (2001).
[32] G. Bertotti, I. D. Mayergoyz, C. Serpico, M. d'Aquino, and R. Bonin, J. Appl. Phys. **105**, 07B712 (2009).
[33] I. D. Mayergoyz, G. Bertotti, and C. Serpico, *Nonlinear Magnetization Dynamics in Nanosystems* (Elsevier, New York, 2009).
[34] H. Suto, K. Kudo, T. Nagasawa, T. Kanao, K. Mizushima, R. Sato, S. Okamoto, N. Kikuchi, and O. Kitakami, Phys. Rev. B **91**, 094401 (2015).
[35] H. Suhl, Proc. IRE **44**, 1270 (1956).
[36] H. Suhl, J. Phys. Chem. Solids **1**, 209 (1957).
[37] P. E. Wigen, *Nonlinear Phenomena and Chaos in Magnetic Materials* (World Scientific, Singapore, 1994).
[38] H. M. Olson, P. Krivosik, K. Srinivasan, and C. E. Patton, J. Appl. Phys. **102**, 023904 (2007).
[39] S. H. Strogatz, *Nonlinear Dynamics and Chaos: With Applications to Physics, Biology, Chemistry, and Engineering*, 2nd ed. (Westview Press, Boulder, Colorado, 2014).
[40] G. Okano and Y. Nozaki, Appl. Phys. Express **8**, 013001 (2015).
[41] G. Okano and Y. Nozaki, Appl. Phys. Express **9**, 063001 (2016).
[42] A. Vansteenkiste, J. Leliaert, M. Dvornik, M. Helsen, F. G. Sanchez, and B. V. Waeyenberge, AIP Adv. **4**, 107133 (2014).
[43] I. Kan, Y. Soeno, T. Roppongi, and Y. Nozaki, Appl. Phys. Lett. **110**, 202404 (2017).
[44] F. B. Mushenok, R. Dost, C. S. Davies, D. A. Allwood, B. J. Inkson, G. Hrkac, and V. V. Kruglyak, Appl. Phys. Lett. **111**, 042404 (2017).
[45] C. S. Davies, V. D. Poimanov, and V. V. Kruglyak, Phys. Rev. B **96**, 094430 (2017).